Real Time Acceleration Tracking of Electro-Hydraulic Shake Tables Combining Inverse Compensation Technique and Neural-Based Adaptive Controller

YU TANG[ID], ZHENCAI ZHU, GANG SHEN, AND WENJUAN ZHANG

School of Mechanical and Electrical Engineering, China University of Mining and Technology, Xuzhou 221116, China
Jiangsu Key Laboratory of Mine Mechanical and Electrical Equipment, China University of Mining and Technology, Xuzhou 221116, China

Corresponding author: Gang Shen (shenganghit@163.com)

ABSTRACT Electro-hydraulic shake table (EHST) is vital seismic testing equipment in earthquake engineering for the assessment of structures subject to dynamic vibration excitations. The EHST system can be generally simplified as an electro-hydraulic servo system with prominent acceleration replication requirement. In order to improve the acceleration tracking performance of a typical EHST system, a novel real-time acceleration tracking strategy combining inverse compensation technique and neural-based adaptive controller is presented in this paper. The traditional three variable controller (TVC) is applied to the EHST system for obtaining a preliminary acceleration tracking accuracy in advance, and then the multi-innovation stochastic gradient algorithm is utilized to estimate the discrete parametric transfer function of the TVC controlled EHST system. Next, the zero magnitude error tracking technique, which is capable of handling non-minimum phase zeros, is exploited to design a stable and casual inverse model, and subsequently the parametric inverse compensation technique for the EHST system is constructed. Finally, a neural-based online adaptive controller is incorporated to the offline designed parametric inverse compensator as an outer loop, and the side effects of the system's inherent nonlinearities, varying dynamics, and external uncertainties are further addressed. The proposed controller is successfully implemented in the control system of a unidirectional EHST test rig using xPC target rapid prototyping technique, and experimental results reveal that a superior acceleration replication performance is achieved in contrast to the other comparative controllers.

INDEX TERMS Electro-hydraulic shake table, acceleration control, inverse compensation, neural-based adaptive control, system identification.

I. INTRODUCTION

Shake tables, also known as earthquake simulators, are applied in experimental testing fields for simulating the vibration circumstances so as to verify the reliability and safety of structures or facilities. Currently, shake tables are extensively utilized in a variety of industrial applications, such as seismic engineering [1], [2], automobile industry [3], [4], earthquake-proof testing [5], [6], etc. Compared with other actuating types, the electro-hydraulic shake table (EHST) is by far the most preferred testing equipment due to the advantages of prominent power density, fast response and large actuating forces [7], [8].

The EHST system can be generally simplified as an electro-hydraulic servo system comprised of a hydraulic cylinder, a servo valve, a moving table and corresponding sensors. The control purpose for shake tables is to real-time replicate the expected acceleration on table. However, high-accuracy acceleration tracking of EHST systems is extremely challenging due to the inherent nonlinear dynamics of the whole control system [9]–[12], such as valve dynamics,

frictions, joint clearance, control-structure interactions, reaction foundation dynamics, etc. Therefore, the acceleration replication accuracy must be adequately improved such that effective reliability assessment for the tested structures or facilities is achieved.

Since the unobservable and marginally unstable modes are always existed in the acceleration measurement process, direct acceleration feedback control of EHST systems is inherently unstable and usually results in unacceptable table drifting phenomenon [13]. To address this problem, displacement of the hydraulic actuator is employed as the feedback signal, and the desired acceleration is transformed to the reference displacement in advance by means of double integrating the acceleration and removing the corresponding drifting components [14]. As for displacement closed-loop control of electro-hydraulic servo systems, considerable efforts ranging from traditional linear methods to modern advanced nonlinear strategies [15]–[20] have been made in this filed for enhancing the displacement tracking accuracy.

Although the acceleration control of EHST systems is based on inner-loop displacement feedback control, there exists differences between the EHST systems and other traditional electro-hydraulic displacement control systems, which makes high accuracy acceleration tracking of EHST systems is inherently different and more difficult. The main reasons are explained as follows: (a) Many neglectable nonlinear factors in traditional electro-hydraulic systems, such as foundation dynamics, tiny mechanical clearances, control-structure interactions etc., have a great influence on the system's acceleration responses, and these factors are difficult to be accurately modeled. (b) The general working frequency bandwidth for acceleration control systems is considerably larger than traditional electro-hydraulic displacement control systems. (c) Acceleration signals are much more sensitive than displacement signals, and the real-time acquired accelerations by accelerometers are always accompanied by bigger noises and disturbances than displacement signals. The existence of the above mentioned factors deteriorate the acceleration replication performance for EHST systems even if a high accuracy inner-loop displacement tracking is achieved. Therefore further outer-loop compensation techniques are essential for acceleration accuracy improvement of EHST systems.

Among all the existed outer-loop compensation techniques, the most celebrated controller for acceleration tracking of EHST systems is the three variable controller (TVC), and it is equipped in the majority of current shake tables as a necessity [21]. To further deal with the nonlinearities in EHST systems, iterative approaches using command shaping principle are extensively investigated. The most famous iterative approach is proposed by Spencer and Yang in [22], where the linearized transfer function of a shake table was firstly established and then the iterative commanding shaping method using inverse transfer function was further presented. De Cuyper *et al.* [23], [24] extended the traditional iterative controller with an feedback controller for the EHST system

in a vibration test rig, and this method substantially improved the convergence property for traditional iterative controllers. Twitchell and Symans [25] described a simplified iterative approach for reproducing the recorded acceleration waveform, and the inverse transfer function pre-filter is directly utilized without iteration steps. Tang *et al.* [26] proposed a combined iterative approach for a multi-axis shake table by introducing an improved internal model controller in the inner loop, and experiments verified the feasibility of the combined strategy in ameliorating the system's varying dynamics.

In addition to the iterative command shaping type approaches, the adaptive controllers, which are capable of dealing with varying dynamics, have also attracted many researcher's interests. The minimal control synthesis (MCS) algorithm was incorporated within both analog and digital controllers for shake tables by Stoten and Gómez [27], and this algorithm was implemented without any parametric knowledge of the system to be controlled. To ameliorate the control performance for conventional MCS controller, variations including feedforward MCS controller [28] and inverse model velocity MCS controller [29] were further developed. Moreover, Yao *et al.* [30] employed the LMS adaptive filtering algorithm to eliminate the phase delay and amplitude attenuation phenomenon for EHST systems with sinusoidal input signal. Seki *et al.* [31] presented an adaptive feedback compensator using an adaptive notch filter for shake tables, and the proposed filter can online identify and compensate for the deteriorative frequency resulted from payload reaction forces. Gang *et al.* [32] applied the online adaptive inverse controller for acceleration tracking of EHST systems, and the performance of different adaptive algorithms were compared in detail.

Recently, some advanced acceleration control techniques for EHST systems have been proposed in literature. For example, Stehman and Nakata [33] described a novel strategy for EHST systems using direct acceleration feedback principle, and force feedback signal is incorporated to prevent the table from drifting. Phillips *et al.* [34] presented a model-based multi-metric control strategy including an offline feed-forward controller and an online feedback controller, where the feedback controller is designed using LQR algorithm. Yang *et al.* [35] developed a hierarchical control scheme comprised of a high-level controller and one or multiple low-level controller, and sliding mode control technique is adopted in the high-level controller for compensating model nonlinearity and uncertainty. Zhang *et al.* [36] presented an adaptive reaching law sliding mode controller for a double EHST system with parameter uncertainties and disturbances. Although these strategies possess the capability of improving control performance for shake tables to some extent, acceleration tracking in a wide bandwidth, especially for high frequency ranges, is still a challenging problem.

In this paper, a novel control strategy using inverse compensation technique and neural-based adaptive controller is proposed to reproduce precise reference acceleration for a typical EHST system. On the basis of traditional

TVC controller, the proposed acceleration strategy employs an parametric inverse compensation technique in inner loop for increasing system's bandwidth and tracking accuracy. The parametric inverse model is designed by multi-innovation stochastic gradient (MISG) algorithm and zero magnitude error tracking (ZMET) technique. In the outer loop, a neural-based adaptive controller is applied to account for the varying dynamics, uncertainties and nonlinearities of the EHST system such that a further acceleration performance improvement is obtained.

The structure of this paper is organized as follows. Section 2 presents the experimental setup of the discussed EHST system and its dynamic model. Section 3 investigates the detailed design procedure for the proposed controller. Section 4 analyzes the experimental performance of the proposed controller. In Section 5, conclusions of this paper are exhibited.
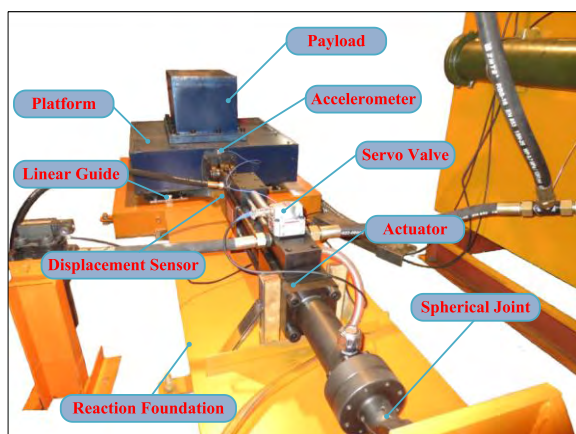

FIGURE 1. Experimental setup of a unidirectional EHST test rig.

II. SYSTEM DESCRIPTION

A. EXPERIMENTAL SETUP

The experimental setup of a unidirectional EHST test rig for evaluation of different control strategies is depicted in Fig. 1, from which it can be observed that a reaction foundation, a hydraulic actuator and a moving platform are included. The reaction foundation is utilized to provide a workable solid anchor for the other components and it is equipped with two parallel linear guides. The moving platform is fixed to the linear guides by bolts and a payload is placed on top of the platform. The hydraulic actuator controlled by a two stage servo-valve is connected to the moving platform and the reaction foundation with spherical joints respectively. To measure acceleration and displacement state information of the EHST test rig, an accelerometer is attached to the end of the actuator's rod and a magnetostrictive displacement sensor is installed beneath the actuator. The detailed technical parameters for the experimental system are exhibited in Table 1, and the main components of the control system are presented in Table 2.

The software architecture for the employed EHST test rig is shown in Fig. 2, where the xPC Target rapid prototyping

TABLE 1. Technical parameters of the experimental system.

Description	Parameter
Platform size	0.8m×0.8m
Payload	150kg
Driving type	Electro-hydraulic
Control mode	Acceleration and position
Actuator stroke	±100mm
Maximum velocity	0.34m/s
Maximum acceleration	2g

TABLE 2. Main components of the control system.

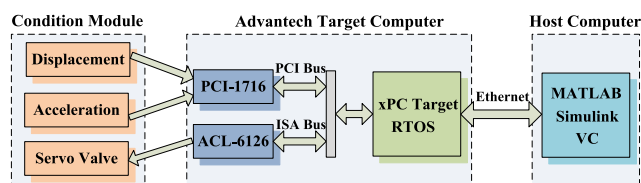| Element	Type	Manufacturer
Actuator	JYQ70/50-200	Weihang
Servo valve	G761-3004b	MOOG
Displacement	1840110200	Germanjet
Accelerometer	3711B112G	PCB
A/D card	PCI1716	Advantech
D/A card	ACL6126	ADlink
Industrial computer	PC610	Advantech

FIGURE 2. Software architecture for the EHST test rig.

technique is employed. The xPC Target environment uses a target computer, separate from a host computer, for running real-time applications. The host computer is a general desktop PC with Microsoft Visual C compiler, MATLAB and Simulink, while the target computer is an Advantech industrial PC with xPC Target real-time operating system, A/D card PCI-1716 and D/A card ACL-6126. The host computer and the target computer are communicated through Ethernet. The displacement and acceleration states are firstly acquired by corresponding sensors, and then sensor outputs are conditioned to voltage signals before they are sent to the target computer. The control output signal is firstly sent out by D/A card in the target computer, and then it is conditioned to the servo valve driving current signal. The control strategies are programmed on the host computer, and the executable code is downloaded from the host computer to the target computer. The sampling time for the EHST test rig is chosen as 0.001s.

B. ELECTRO-HYDRAULIC SHAKE TABLE MODELING

As shown in Fig. 3, the principle of the discussed EHST test rig can be simplified in the form of a double ended hydraulic actuator controlled by a three-land-four-way servo
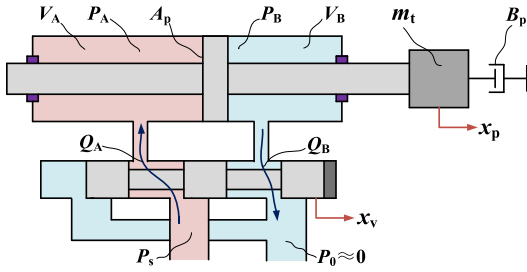
FIGURE 3. Simplified principle for EHST modeling.

valve. Hence, the linearized load flow Q_L for the servo valve can be expressed as [37]

$$Q_L = K_q x_v - K_c P_L \tag{1}$$

where x_v is the valve spool displacement, P_L is the pressure drop across the load defined as $P_L = P_A - P_B$, K_q and K_c are the linearized flow gain and flow pressure coefficient respectively, which can be written in the form of

$$K_q = \frac{\partial Q_L}{\partial x_v} = C_d w_v \sqrt{\frac{P_s - \frac{x_v}{|x_v|} P_L}{\rho}} \tag{2}$$

$$K_c = -\frac{\partial Q_L}{\partial P_L} = C_d w_v |x_v| \sqrt{\frac{1}{4\rho(P_s - \frac{x_v}{|x_v|} P_L)}} \tag{3}$$

where C_d is the discharge coefficient, w_v is the valve orifices constant area gradient, ρ is the oil density, P_s is the system supply pressure.

Taking oil compressibility, internal leakage, external leakage and chamber volume variation into consideration, the flow for each chamber of the hydraulic actuator can be described as

$$\begin{cases} Q_A = A_p \dfrac{dx_p}{dt} + C_{ip}P_L + C_{ep}P_A + \dfrac{V_{A0} + A_p x_p}{\beta_e} \dfrac{dP_A}{dt} \\ Q_B = A_p \dfrac{dx_p}{dt} + C_{ip}P_L - C_{ep}P_B - \dfrac{V_{B0} - A_p x_p}{\beta_e} \dfrac{dP_B}{dt} \end{cases} \tag{4}$$

where A_p is the actuator's actuating area, x_p is the actuator's displacement, C_{ip} is the internal leakage coefficient, C_{ep} is the external leakage coefficient, β_e is the oil effective bulk modulus, V_{A0} and V_{B0} are the initial left and right chamber volume respectively.

Generally the actuator's piston of the EHST system is centered in initial state, which indicates that the initial left and right chamber volumes are identical to each other, and hence (4) can be further simplified as

$$Q_L = A_p \frac{dx_p}{dt} + C_{tp}P_L + \frac{V_t}{4\beta_e} \frac{dP_L}{dt} \tag{5}$$

where V_t is the total chamber volume, C_{tp} is the total leakage coefficient defined as $C_{tp} = C_{ip} + C_{ep}/2$.

Ignoring hydraulic oil mass and actuator's friction, the force balance equation of the EHST system can be expressed as

$$m_t \frac{d^2 x_p}{dt^2} = P_L A_p - B_p \frac{dx_p}{dt} \tag{6}$$

where m_t is the total equivalent mass referred to piston, B_p is the viscous damping coefficient.

Employing the Laplace transformation to both sides of (1), (5), (6) and simplifying, the open-loop transfer function $G_{dp}(s)$ from valve displacement to actuator's displacement can be derived as follows

$$G_{dp}(s) = \frac{K_0}{s\left(\frac{s^2}{\omega_h^2} + \frac{2\xi_h}{\omega_h}s + 1\right)} \tag{7}$$

where K_0 is the system's flow gain represented by $K_0 = K_q/A$, ω_h is the system's natural angular frequency defined as $\omega_h = \sqrt{4\beta_e A^2/(V_t m)}$, ξ_h is the system's damping ratio expressed as $\xi_h = (K_c + C_{tp})\sqrt{\beta_e m/V_t}/A$.

III. CONTROLLER DESIGN

The overall control principle of the proposed controller is presented in Fig. 4. As can be obviously observed from Fig. 4, the proposed controller is comprised of three components including traditional TVC controller, inverse compensation controller and neural-based adaptive controller. The traditional TVC controller is firstly exploited in the inner displacement loop to stabilize the EHST system with an elementary acceleration replication accuracy. Next, to construct the stable inverse feedforward model for the inverse compensation controller, MISG algorithm is utilized to identify the discrete transfer function of the EHST system, and ZMET technique is brought in to deal with the existing NMP zeros. Finally the neural-based adaptive controller is combined with the inverse compensation controller to account for the system's varying dynamics, uncertainties and nonlinearities.
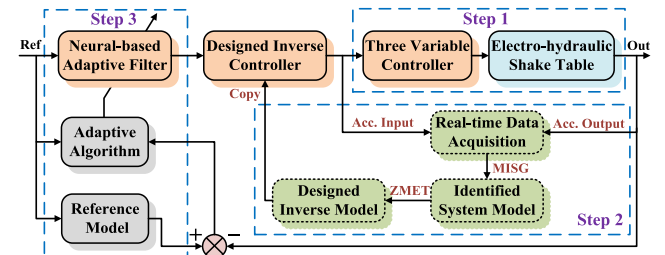

FIGURE 4. Control scheme of the proposed algorithm for EHST system.

A. TRADITIONAL THREE VARIABLE CONTROLLER

The TVC controller is the most celebrated strategy for acceleration control of EHST systems and it is extensively utilized in industrial applications to achieve a preliminary acceleration tracking performance. The theory behind the TVC controller is based on zero-pole placement principle and the working scheme of the TVC controller is presented in Fig. 5. As can be seen from Fig. 5, the TVC controller is constructed by TVC feedforward and feedback controllers. The TVC feedback controller consists of displacement, velocity and acceleration feedback signals, where the displacement signal is utilized to stabilize the whole
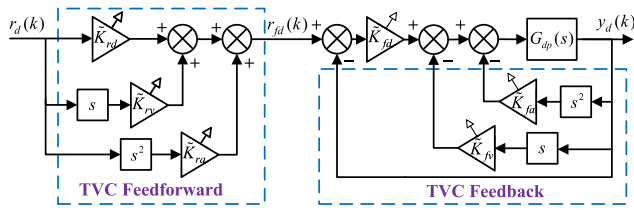
FIGURE 5. Working scheme of TVC controller for EHST system

closed-loop system, the velocity signal is adopted for increasing system's intrinsic frequency, and the acceleration signal serves the purpose of improving the system's damping ratio. The displacement and acceleration signals are directly acquired by corresponding sensors, while the velocity signal is manually synthesized by using the displacement signal in low frequency bandwidth and the acceleration signal in high frequency bandwidth.

Referring to Fig. 5, the transfer function $G_{FB}(s)$ from the feedforward displacement signal $r_{fd}(k)$ to the system's output displacement signal $y_d(k)$ can be simplified as follows

$$G_{FB}(s) = \frac{\tilde{K}_{fd}K_0}{\frac{s^3}{\omega_h^2} + \left(\tilde{K}_{fa}K_0 + 2\frac{\xi_h}{\omega_h}\right)s^2 + (\tilde{K}_{fv}K_0 + 1)s + \tilde{K}_{fd}K_0} \tag{8}$$

With the implementation of TVC feedback controller, the desired system transfer function $G_{dFB}(s)$ can be described as

$$G_{dFB}(s) = \frac{1}{\left(\frac{s}{\omega_r} + 1\right)\left(\frac{s^2}{\omega_{nc}^2} + 2\frac{\xi_{nc}}{\omega_{nc}}s + 1\right)} \tag{9}$$

where ω_r is the desired system displacement bandwidth, ω_{nc} is generally selected as $\omega_{nc} = 1.05\omega_h \sim 1.2\omega_h$ and $\xi_{nc} \approx 0.7$.

Equating the right sides of (8)-(9) and simplifying, the ideal TVC feedback parameters can be deduced as

$$\begin{cases} \tilde{K}_{fd} = \dfrac{\omega_r \omega_{nc}^2}{K_0 \omega_h^2} \\ \tilde{K}_{fv} = \dfrac{2\xi_{nc}\omega_r\omega_{nc}}{K_0\omega_h^2} + \dfrac{\omega_{nc}^2}{K_0\omega_h^2} - \dfrac{1}{K_0} \\ \tilde{K}_{fa} = \dfrac{2\xi_{nc}\omega_{nc}}{K_0\omega_h^2} + \dfrac{\omega_r}{K_0\omega_h^2} - \dfrac{2\xi_h}{K_0\omega_h} \end{cases} \tag{10}$$

The TVC feedforward controller, which is comprised of displacement, velocity and acceleration feedforward signals, is utilized for bandwidth extension and a higher tracking accuracy. Employing the TVC feedforward controller, the system's transfer function from reference displacement signal $r_d(k)$ to the output displacement signal $y_d(k)$ can be written as

$$G_{FF}(s) = \frac{y_d(k)}{r_d(k)} = \frac{\tilde{K}_{ra}s^2 + \tilde{K}_{rv}s + \tilde{K}_{rd}}{\left(\frac{s}{\omega_r} + 1\right)\left(\frac{s^2}{\omega_{nc}^2} + 2\frac{\xi_{nc}}{\omega_{nc}}s + 1\right)} \tag{11}$$

The basic principle for TVC feedforward controller is to eliminate the system poles close to imaginary axis, and therefore the TVC feedforward parameters can be deduced as follows

$$\begin{cases} \tilde{K}_{rd} = 1 \\ \tilde{K}_{rv} = 2\xi_{nc}/\omega_{nc} \\ \tilde{K}_{ra} = 1/\omega_{nc}^2 \end{cases} \tag{12}$$

As for the reference displacement signal, it is computed by a reference signal generator with the principle of double integrating the acceleration signal and removing the drifting components. The transfer function for the signal generator $G_{ref}(s)$ can be expressed in the form of

$$G_{ref}(s) = \frac{r_d(k)}{r_a(k)} = \frac{K_{ref}}{d_f\left(\frac{s^2}{\omega_{ref}^2} + 2\frac{\xi_{ref}}{\omega_{ref}}s + 1\right)} \tag{13}$$

where $K_{ref} = 1$, $\omega_{ref} = 0.5$Hz, $\xi_{ref} = 0.6$ and $d_f = \omega_{ref}^2$ are selected to prevent the EHST system from exceeding the actuator's maximum stroke in relatively low frequency.

B. Parametric Inverse Compensation Technique

The parametric inverse compensation technique for EHST system is implemented to improve the acceleration tracking accuracy of traditional TVC controller, and the general scheme for the inverse compensation technique is demonstrated in Fig. 6. As can be observed from Fig. 6, the parametric inverse compensation technique is comprised of two steps. The first step is to estimate the closed-loop system model, and the next is to offline design the parametric feedforward inverse model.
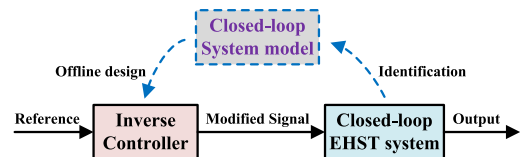

FIGURE 6. Scheme for the parametric inverse compensation technique.

As for the first step of the parametric inverse compensation controller, the controlled auto-regressive (CAR) model is exploited to represent the whole acceleration system controlled by traditional TVC controller, and the CAR model can be described in the form of

$$A(z^{-1})y(k) = z^{-d}B(z^{-1})u(k) + v(k) \tag{14}$$

where $u(k)$ and $y(k)$ are the system's input and output respectively, $v(k)$ is a stochastic white noise with zero mean, d is the pure time delay, z^{-1} is the backward shift operator, $A(z^{-1})$ and $B(z^{-1})$ are polynomials expressed as

$$\begin{cases} A(z^{-1}) = 1 + a_1 z^{-1} + \cdots + a_n z^{-n_a} \\ B(z^{-1}) = b_0 + b_1 z^{-1} + \cdots + b_n z^{-n_b}(b_0 \neq 0, n_b \leq n_a) \end{cases} \tag{15}$$

Substituting (15) into (14) and simplifying, the linear regression model for estimation of the acceleration system is concluded as follows

$$y(k) = \boldsymbol{\varphi}^T(k)\boldsymbol{\theta} + v(k) \tag{16}$$

where $\boldsymbol{\varphi}(k)$ is the vector consisting of the system's input-output data, $\boldsymbol{\theta}$ is the coefficient vector to be determined, $\boldsymbol{\varphi}(k)$ and $\boldsymbol{\theta}$ are respectively defined as

$$\begin{cases} \boldsymbol{\varphi}(k) = [-y(k-1), \cdots, -y(k-n_a), u(k-d), \cdots, \\ \qquad u(k-d-n_b)]^T \\ \boldsymbol{\theta} = [a_1, a_2, \cdots, a_{n_a}, b_0, b_1, \cdots, b_{n_b}]^T \end{cases} \tag{17}$$

and then the identification procedure is transformed to compute vector $\boldsymbol{\theta}$ with acquired input-output acceleration data.

To obtain the coefficient vector of the system's transfer function, the MISG algorithm [38] using both current and past data at each iteration is employed. The basic principle for MISG algorithm is to expand the scalar innovation to an innovation vector (i.e. multi-innovation), and the innovation vector $\boldsymbol{E}(p, t)$ is selected as

$$\boldsymbol{E}(p, k) = \begin{bmatrix} y(k) - \boldsymbol{\varphi}^T(k)\hat{\boldsymbol{\theta}}(k-1) \\ y(k-1) - \boldsymbol{\varphi}^T(k-1)\hat{\boldsymbol{\theta}}(k-1) \\ \vdots \\ y(k-p+1) - \boldsymbol{\varphi}^T(k-p+1)\hat{\boldsymbol{\theta}}(k-1) \end{bmatrix}_{p \times 1}$$
$$= \boldsymbol{Y}(p, k) - \boldsymbol{\Phi}^T(p, k)\hat{\boldsymbol{\theta}}(k-1) \tag{18}$$

where p is the innovation length, $\hat{\boldsymbol{\theta}}(k)$ is the estimated coefficient vector at kth step, $\boldsymbol{\Phi}(p, k)$ is the information matrix, $\boldsymbol{Y}(p, k)$ is the stacked acceleration output vector, $\boldsymbol{\Phi}(p, k)$ and $\boldsymbol{Y}(p, k)$ are respectively defined as follows

$$\begin{cases} \boldsymbol{\Phi}(p, k) = [\boldsymbol{\varphi}(k), \boldsymbol{\varphi}(k-1), \cdots, \boldsymbol{\varphi}(k-p+1)] \\ \boldsymbol{Y}(p, k) = [y(k), y(k-1), \cdots, y(k-p+1)]^T \end{cases} \tag{19}$$

and the recursive steps for MISG algorithm is given as follows

$$\begin{cases} \hat{\boldsymbol{\theta}}(k) = \hat{\boldsymbol{\theta}}(k-1) + \dfrac{\boldsymbol{\Phi}(p, k)}{r(k)}\boldsymbol{E}(p, k) \\ \boldsymbol{E}(p, k) = \boldsymbol{Y}(p, k) - \boldsymbol{\Phi}^T(p, k)\hat{\boldsymbol{\theta}}(k-1) \\ r(k) = r(k-1) + \|\boldsymbol{\varphi}(k)\|^2 \end{cases} \tag{20}$$

where $1/r(k)$ is the convergence factor and $r(0)$ is chosen as $r(0) = 1$, the norm of vector $\boldsymbol{\varphi}(k)$ is defined as $\|\boldsymbol{\varphi}(k)\|^2 = \text{tr}[\boldsymbol{\varphi}(k)\boldsymbol{\varphi}^T(k)]$.

Employing the MISG algorithm presented in (20), the parametric acceleration model for traditional TVC controlled EHST system can be easily identified, and the next step is to design a feasible inverse compensator for the previous estimated transfer function. As sampling holders are inevitably existed in industrial control systems and the hydraulic actuator is physically non-collocated, the identified system transfer function always involves NMP zeros (i.e. zeros outside the unit circle), and this phenomenon will result in an unstable inverse controller if denominator and numerator of the identified model are directly exchanged. To solve this problem,

the ZMET technique [39] is exploited to guarantee a stable inverse controller. The first step of ZMET technique is to separate the estimated system model $\hat{G}_a(z)$ into two parts as follows

$$\hat{G}_a(z) = \frac{\hat{B}(z)}{\hat{A}(z)} = \frac{\hat{B}_{\text{MP}}(z)\hat{B}_{\text{NMP}}(z)}{\hat{A}(z)} \tag{21}$$

where $\hat{A}(z)$ is the denominator of identified acceleration system transfer function, $\hat{B}(z)$ is the numerator of identified system transfer function, $\hat{B}_{\text{MP}}(z)$ is the polynomials with all MP zeros, $\hat{B}_{\text{NMP}}(z)$ is the polynomials with all NMP zeros. $\hat{B}_{\text{NMP}}(z)$ can be further described as

$$\hat{B}_{\text{NMP}}(z) = \hat{b}_{n0} + \hat{b}_{n1}z + \cdots + \hat{b}_{nn}z^n \tag{22}$$

where n equals to the numbers of NMP zeros.

The ZMET technique utilizes all-pass filter principle to convert all the existed NMP zeros inside the unit circle, and the transformed MP polynomial $\hat{B}^*_{\text{NMP}}(z)$ with respect to $\hat{B}_{\text{NMP}}(z)$ can be expressed as

$$\hat{B}^*_{\text{NMP}}(z) = \hat{b}_{n0}z^n + \hat{b}_{n1}z^{n-1} + \cdots + \hat{b}_{nn} \tag{23}$$

Employing (23), the offline designed stable inverse model $\hat{G}^{-1}_{ad}(z)$ for the identified acceleration transfer function $\hat{G}_a(z)$ can be written as follows

$$\hat{G}^{-1}_{ad}(z) = \frac{\hat{A}(z)}{z^s \hat{B}_{\text{MP}}(z)\hat{B}^*_{\text{NMP}}(z)} \tag{24}$$

where delay z^s is combined to ensure causality of the designed inverse model.

With the offline designed stable inverse model, the detailed block diagram of parametric inverse compensation technique for EHST system is presented in Fig. 7. Simplifying the block diagram of Fig. 7, the system's output and acceleration tracking error can be deduced as

$$\begin{cases} y_a(k) = \hat{G}^{-1}_{ad}(z)\hat{G}_a(z)(1 + \Delta G_a)r_a(k) \\ e_a(k) = [1 - \hat{G}^{-1}_{ad}(z)\hat{G}_a(z)(1 + \Delta G_a)]r_a(k) \end{cases} \tag{25}$$

where ΔG_a is multiplicative modeling error between the estimated and actual TVC controlled EHST system.
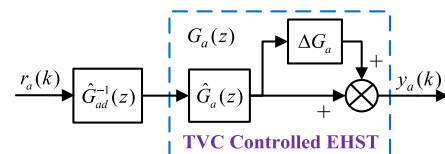

FIGURE 7. Block diagram for parametric inverse compensation technique.

As can be inferred from (25), if the multiplicative modeling error and the inverse model design error are sufficiently small (i.e. $\Delta G_a \approx 0$ and $\hat{G}^{-1}_{ad}(z)\hat{G}_a(z) \approx 1$), the acceleration output will perfectly replicate the reference input signal. Unfortunately, for the sake of system's varying dynamics, uncertainties and nonlinearities, the multiplicative modeling error is inevitably existed in the EHST system.
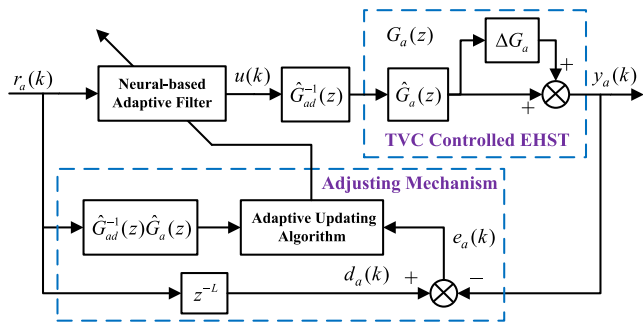
FIGURE 8. The proposed control architecture for EHST system.

Moreover, the ZMET technique is bound to bring in phase lag error during the inverse model design procedure. Hence, these defects should also be addressed so as to obtain a higher acceleration replication performance for the EHST system.

C. NEURAL-BASED ADAPTIVE CONTROLLER
To deal with the disadvantages of parametric inverse compensation technique, a neural-based adaptive controller is further applied to the EHST system, and the architecture of the proposed controller is exhibited in Fig. 8. As can be observed from Fig. 8, the neural-based adaptive controller is working in outer loop of the EHST system to compensate for the system's variation, nonlinearity and disturbances, and it is comprised of a neural-based adaptive filter and an online adjusting mechanism.
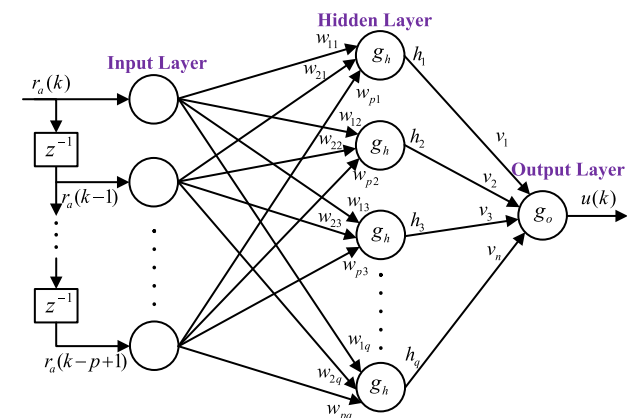

FIGURE 9. The detailed scheme for neural-based adaptive filter.

The detailed scheme for the neural-based adaptive filter is presented in Fig. 9, where three layers including the input layer, hidden layer and output layer are required. As shown in Fig. 9, a tapped delay line (TDL) of the desired acceleration signal is firstly injected to the input nodes, and then the input data sequence is processed in the hidden layer by weight coefficients. The output of the hidden neural node $h_j(k)$ can

be described by the following relation

$$h_j(k) = g_h[net_h^j(k)]$$
$$= g_h\left(\sum_{i=1}^{p} w_{ij}(k)r_a(k-i+1)\right) \quad (i=1,\cdots,p) \quad (26)$$

where $g_h(\cdot)$ is the activation function for hidden neural node, $net_h^j(k)$ is the input of hidden neural node, $w_{ij}(k)$ is the parameter weight between the ith neural node of the input layer and the jth neural node of the hidden layer, p is the numbers of the input layer nodes.

Similarly, the output $u(k)$ for the output neural node can be expressed as follows

$$u(k) = g_o[net_o(k)] = g_o\left(\sum_{j=1}^{q} h_j(k)v_j(k)\right) \quad (j=1,\cdots,q)$$
$$(27)$$

where $g_o(\cdot)$ is the activation function for output neural node, $net_o(k)$ is the input for output neural node, $v_j(k)$ is the parameter weight between the jth neural node of the hidden layer and the neural node of the output layer, q is the numbers of the hidden layer nodes.

To obtain the adaptive updating law for the neural-based filter weights, defining the desired acceleration output as $d_a(k)$ and referring to Fig. 8, the acceleration tracking error $e_a(k)$ can be written as

$$e_a(k) = r_a(k)z^{-n} - u(k)\hat{G}_{ad}^{-1}(z)\hat{G}_a(z)(1+\Delta G_a) \quad (28)$$

and then the error cost function $J(k)$ to be minimized for the EHST system is selected as follows

$$J(k) = \frac{1}{2}\left[r_a(k)z^{-n} - u(k)\hat{G}_{ad}^{-1}(z)\hat{G}_a(z)(1+\Delta G_a)\right]^2 \quad (29)$$

Combining (26), (27), (29) and simplifying, the gradient of cost function $J(k)$ with respect to $v_j(k)$ and $w_{ij}(k)$ can be respectively deduced as follows

$$\frac{\partial J(k)}{\partial v_j(k)} = \frac{\partial J(k)}{\partial u(k)}\frac{\partial u(k)}{\partial net_o(k)}\frac{\partial net_o(k)}{\partial v_j(k)}$$
$$= -e_a(k)\hat{G}_{ad}^{-1}(z)\hat{G}_a(z)(1+\Delta G_a)g_o'[net_o(k)]h_j(k)$$
$$(30)$$

$$\frac{\partial J(k)}{\partial w_{ij}(k)} = \frac{\partial J(k)}{\partial h_j(k)}\frac{\partial h_j(k)}{\partial net_h^j(k)}\frac{\partial net_h^j(k)}{\partial w_{ij}(k)}$$
$$= \left(\frac{\partial J(k)}{\partial u(k)}\frac{\partial u(k)}{\partial net_o(k)}\frac{\partial net_o(k)}{\partial h_j(k)}\right)\frac{\partial h_j(k)}{\partial net_h^j(k)}\frac{\partial net_h^j(k)}{\partial w_{ij}(k)}$$
$$= \left\{\begin{array}{l} -e_a(k)\hat{G}_{ad}^{-1}(z)\hat{G}_a(z)(1+\Delta G_a)g_o'[net_o(k)] \\ v_j(k)g_h'[net_h^j(k)]r_a(k-i+1) \end{array}\right\}$$
$$(31)$$

and then the online weight updating law for $v_j(k)$ and $w_{ij}(k)$ can be expressed as

$$\begin{cases} v_j(k+1) = v_j(k) - \eta e_a(k)\dfrac{\partial J(k)}{\partial v_j(k)} \\ w_{ij}(k+1) = w_{ij}(k) - \eta e_a(k)\dfrac{\partial J(k)}{\partial w_{ij}(k)} \end{cases} \qquad (32)$$

where η is the updating step size for $v_j(k)$ and $w_{ij}(k)$.

To prevent the saturation problem caused by traditional sigmoid or hyperbolic activation functions and to simplify the updating process, the following activation functions for hidden and output nodes are selected

$$\begin{cases} g_h[net_h^j(k)] = net_h^j(k) \\ g_o[net_o(k)] = net_o(k) \end{cases} \qquad (33)$$

Substituting (33) into (32) and neglecting the system's multiplicative error ΔG_a, the final adaptive updating law for the weights of neural-based filter can be concluded as

$$\begin{cases} v_j(k+1) = v_j(k) + \eta e_a(k)\hat{G}_{ad}^{-1}(z)\hat{G}_a(z)h_j(k) \\ w_{ij}(k+1) = w_{ij}(k) + \eta e_a(k)\hat{G}_{ad}^{-1}(z)\hat{G}_a(z) \\ \qquad\qquad \times v_j(k)r_a(k-i+1) \end{cases} \qquad (34)$$

As shown in (30) and (31), to compute the instantaneous gradient for updating the weights of the neural-based filter for the proposed controller, the reference input acceleration signal must be firstly filtered by the EHST system using the parametric inverse compensation technique. However, due to the fact that the actual model $\hat{G}_{ad}^{-1}(z)\hat{G}_a(z)(1 + \Delta G_a)$ itself is not available in physical implementation situation, an estimation of the system model $\hat{G}_{ad}^{-1}(z)\hat{G}_a(z)$ is applied in (34). As for the stability analysis of the proposed controller, it is similar to the well-known filtered least mean square algorithm[40], and the phase error of the estimated system model $\hat{G}_{ad}^{-1}(z)\hat{G}_a(z)$ for the EHST system using parametric inverse compensation technique must satisfy the following requirement

$$\left| \angle \hat{G}_{ad}^{-1}(z)\hat{G}_a(z)(1 + \Delta G_a) - \angle \hat{G}_{ad}^{-1}(z)\hat{G}_a(z) \right| < 90° \qquad (35)$$

It can be easily indicated from (35) that the estimated system model $\hat{G}_{ad}^{-1}(z)\hat{G}_a(z)$ should be accurate to within 90° of phase in comparison to the actual EHST system so as to guarantee the stability of the proposed controller. Conversely, if the estimated model $\hat{G}_{ad}^{-1}(z)\hat{G}_a(z)$ is incorrect by more than 90° during the bandwidth of the tested acceleration input signal, the weights of the neural-based filter for the proposed controller will update in the wrong direction, which will result in the divergence of the whole control system.

IV. EXPERIMENTAL RESULTS AND DISCUSSION

To verify the feasibility of the proposed controller, experiments are implemented on the established EHST test rig in Fig. 1. The traditional TVC controller is firstly utilized for primitive acceleration control accuracy of the EHST system, and the TVC parameters are online tuned with trial and error method. During the tuning process of the TVC
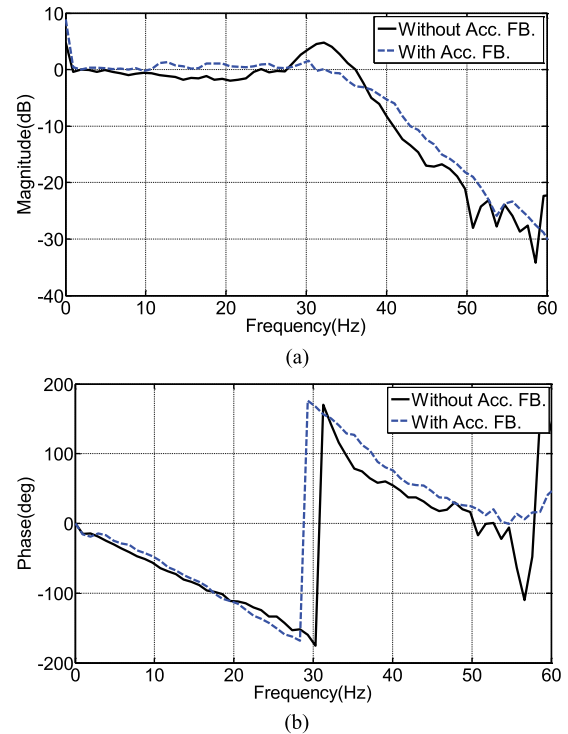

FIGURE 10. Displacement frequency characteristics of EHST system. **(a) Magnitude characteristics. (b) Phase characteristics.**

controller, the system's time and frequency domain responses are carefully observed respectively, and the eventual online well-tuned TVC parameters are listed in Table 3. It is worth noting that the velocity feedback signal is omitted in the TVC feedback controller, and this is for the reason that an appropriate displacement natural frequency is already obtained when acceleration and displacement feedback signals are utilized.

TABLE 3. The eventual tuned TVC parameters for EHST.

Description	Symbol	Value
Displacement feedback	$\tilde{K}_{fd}$	22.5
Velocity feedback	$\tilde{K}_{fv}$	0
Acceleration feedback	$\tilde{K}_{fa}$	0.025
Displacement feedforward	$\tilde{K}_{rd}$	1
Velocity feedforward	$\tilde{K}_{rv}$	0.84
Acceleration feedforward	$\tilde{K}_{ra}$	0.00053

To indicate the functionality of acceleration feedback control, the corresponding displacement frequency characteristics for closed-loop control of the EHST system is exhibited in Fig. 10, and the characteristics without acceleration feedback is also presented for a comparative purpose. As can be seen from Fig. 10, with the implementation of acceleration feedback, the hydraulic resonance appeared at frequency 32Hz is effectively eliminated due to the increasement of system's damping ratio, and therefore a more satisfactory displacement performance is achieved.

The TVC feedforward controller is exploited on basis of the acceleration closed-loop for EHST system, and the experimental acceleration frequency characteristics with and
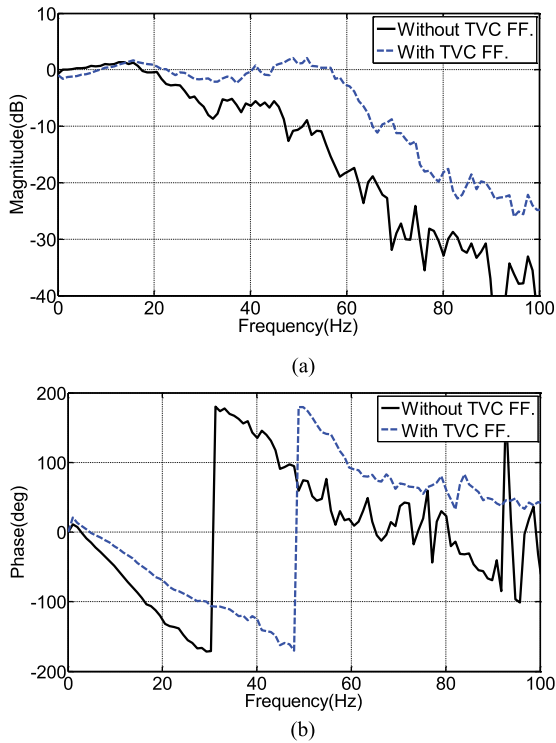
**FIGURE 11. Acceleration frequency characteristics of EHST system.
(a) Magnitude characteristics. (b) Phase characteristics.**

without TVC feedforward controller is presented in Fig. 11. As can be inferred from Fig. 11, the acceleration performance by TVC feedforward controller is remarkably ameliorated in contrast to the system without TVC feedforward compensation in terms of both magnitude and phase frequency responses. Specifically, after employing the TVC feedforward controller, the acceleration system bandwidth is extended from initial 26Hz to nearly 60Hz (-3dB criterion) and the system's phase delay phenomenon is reduced from initial 15Hz to 20Hz ($-90°$ criterion).

For the purpose of identifying the system model by TVC controller, a random acceleration signal with amplitude 0.5g and frequency 2-100Hz is selected as the excitation signal, and the corresponding acceleration input-output data are real-time acquired. Taking the model complexity, estimation precision, and computational load into consideration, a 6-order CAR model is chosen to represent the acceleration system by continuously attempts, and the final estimated discrete system model using the MISG algorithm can be written as

$$\hat{G}_a(z) = \frac{\left\{ \begin{array}{l} -0.0028226(z-3.345)(z-0.9055) \\ (z^2-1.842z+0.949)(z^2-1.636z+2.158) \end{array} \right\}}{\left\{ \begin{array}{l} (z^2-1.88z+0.8915)(z^2-1.849z+0.9435) \\ (z^2-1.823z+0.9406) \end{array} \right\}}$$
(36)

It can be obviously observed from (36) that the estimated discrete system has three NMP zeros outside the unit circle, i.e. $z = 3.345$ and $z = 0.8187 \pm 1.220$ i, and these

unstable zeros must be handled in the inverse design process. With implementation of the ZMET technique, the offline designed stable and casual inverse transfer function can be described as

$$\hat{G}_{ad}^{-1}(z) = \frac{\left\{ \begin{array}{l} (z^2-1.88z+0.8915)(z^2-1.849z+0.9435) \\ (z^2-1.823z+0.9406) \end{array} \right\}}{\left\{ \begin{array}{l} -0.0028226(-3.345z+1)(z-0.9055) \\ (z^2-1.842z+0.949)(2.158z^2-1.636z+1) \end{array} \right\}}$$
(37)

To verify the feasibility of the MISG identification algorithm and the ZMET technique, the frequency characteristics of identified and designed inverse model for the EHST system is presented in Fig. 12, and the experimental characteristics is also exhibited for illustration purpose. As can be observed from Fig. 12, the estimated system model by MISG algorithm is in high accordance with the experimental model calculated by H1 method during the whole frequency range. Moreover, the designed inverse model using ZMET technique shows an ideal magnitude property and an acceptable phase characteristics compared with the offline identified acceleration model within the interested frequency bandwidth.

With the feasible inverse model, the feedforward strategy using parametric inverse compensation technique is established by cascading the designed model to the TVC controlled EHST system. Similar to the system identification process, a broad bandwidth random signal is utilized to excite the system, and the final frequency characteristics of the EHST system with parametric inverse compensator is exhibited in Fig. 13, where the traditional TVC controller is selected as a comparison.

As illustrated by Fig. 13, the parametric inverse compensation technique can effectively enhance the system's acceleration tracking performance in the aspects of both magnitude and phase characteristics, and the magnitude and phase bandwidth are increased by 66.67% (from initial 60Hz to 100Hz) and 148% (from initial 25Hz to 62Hz), respectively. Besides, the magnitude property with parametric inverse compensator is much closer to the 0dB line in contrast to that of the TVC controller, and this also reveals that a smaller magnitude tracking error is achieved by the parametric inverse compensation technique.

On the basis of parametric inverse compensation technique, the proposed controller for the discussed EHST system is constructed by introducing a neural-based adaptive controller. For stability analysis of the proposed controller, the phase characteristics of the estimated system model $\hat{G}_{ad}^{-1}(z)\hat{G}_a(z)$ and the actual system model $\hat{G}_{ad}^{-1}(z)\hat{G}_a(z)$ $(1 + \Delta G_a)$ is presented in Fig. 14, where the estimated phase is calculated by the identified $\hat{G}_a(z)$ and the designed $\hat{G}_{ad}^{-1}(z)$, while the actual system phase is computed using the experimental results of the system controlled by parametric inverse compensator. As for the phase mismatch error between the estimated and actual system, it can be observed from Fig. 14 that the maximum phase error is nearly 22° at frequency 52Hz, and the stability criterion described in (35)
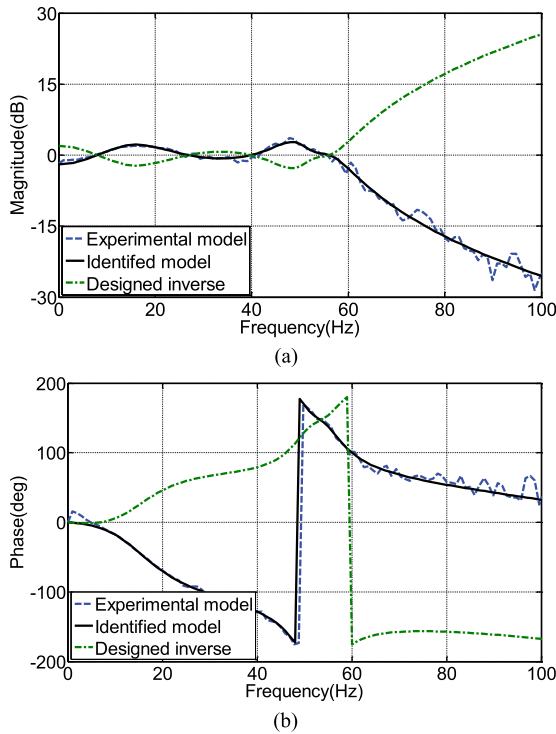
FIGURE 12. Frequency characteristics of identified and designed model.
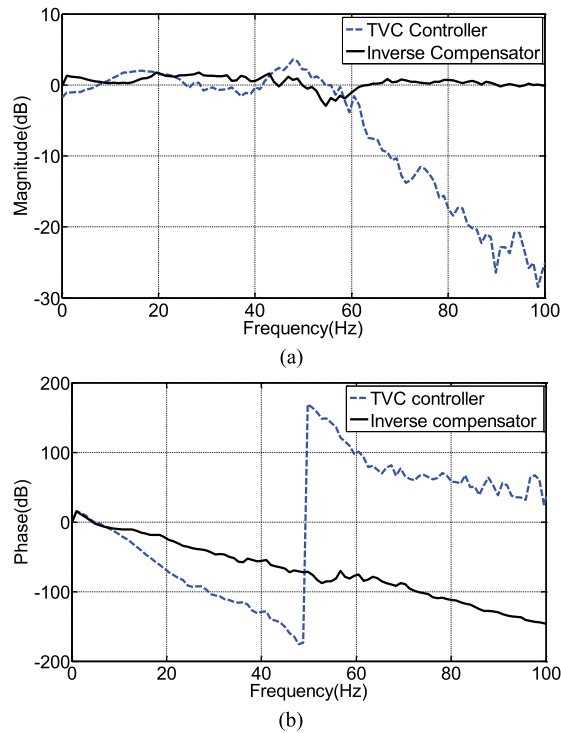(a) Magnitude characteristics. (b) Phase characteristics.

FIGURE 13. Frequency characteristics by TVC and parametric inverse compensator. (a) Magnitude characteristics. (b) Phase characteristics.

is satisfied during the whole frequency bandwidth. Therefore, the stability of the proposed controller for the EHST system is guaranteed.
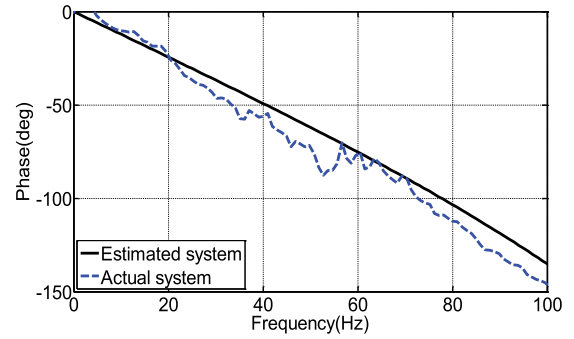

FIGURE 14. Phase characteristics for stability analysis of the proposed controller.

During the implementation of the proposed controller, 8 input neural nodes and 10 hidden neural nodes are firstly selected by trial and error method. As the proposed controller requires an online training process to tune the neural-based filter weights in advance, a random acceleration signal with amplitude 0.5g and frequency range 2-45Hz is adopted for that purpose. After the weights of the neural-based filter are well trained, these parameters are further utilized as the initial values for the eventual tested acceleration waveforms.

The first tested acceleration signal for evaluation of different controllers is a random signal with magnitude 0.5g and frequency 2-30Hz, and time-history waveform of the selected random signal is presented in Fig. 15. Applying the reference random acceleration signal to the unidirectional EHST test rig, the real-time experimental acceleration tracking results of different controllers are obtained, and then the partial enlargement for acceleration waveforms with different controllers is exhibited in Fig. 16.
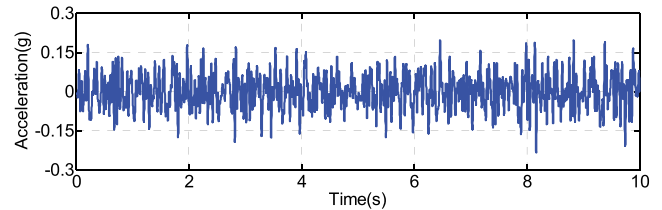

FIGURE 15. Random reference acceleration signal for EHST system.

As can be observed from Fig. 16, the acceleration tracking performance for traditional TVC controller is the worst among the three adopted controllers, and the corresponding output acceleration exhibits both large delay error and magnitude tracking error. With implementation of the parametric inverse compensator, the most significant improvement is the reduction of the system's phase delay error. Although the magnitude tracking error is also alleviated to a certain degree by the parametric inverse compensator, it still needs to be further improved. As far as the proposed controller is concerned, the magnitude tracking error is remarkably reduced as an online adaptive controller is combined, and the adaptive
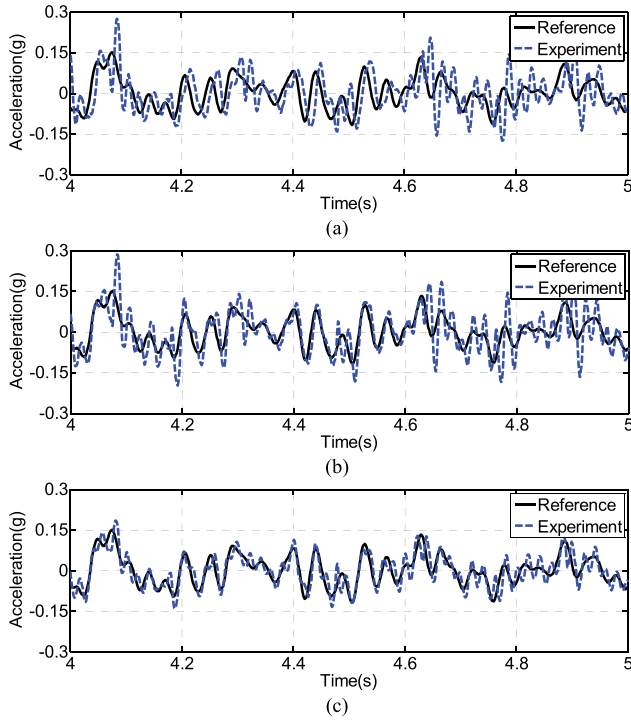
FIGURE 16. Partial enlargement for different controllers with random input. (a) TVC controller. (b) Parametric inverse compensator. (c) Proposed controller.
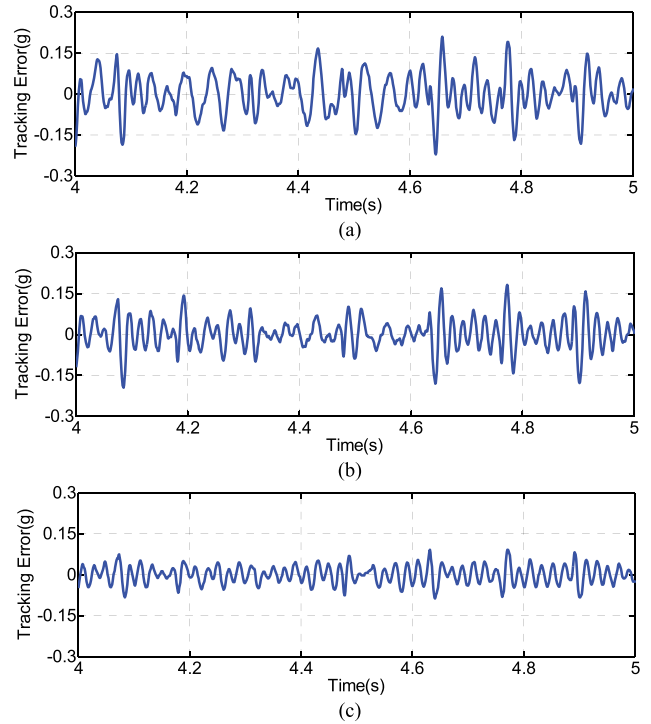

FIGURE 17. Tracking error of different controllers with random input. (a) TVC controller. (b) Parametric inverse compensator. (c) Proposed controller.

controller is capable of dealing with the inverse compensator's defects in terms of modeling error, disturbances and uncertainties. Similar conclusions can also be obtained from Fig. 17, in which the corresponding acceleration tracking error with respect to Fig. 16 is presented.

Objective performance evaluation of different controllers for EHST systems should be one of the cornerstones in scientific research [41], [42], and for this purpose the relative root mean square error (RMSE) and the relative maximum error (RME) are chosen as the quantitative evaluation indexes. The computation formulations for the RMSE index and the RME error are described as

$$\text{RMSE} = \frac{\sqrt{\sum\limits_{i=1}^{M} [r_a(k) - y_a(k)]^2 / M}}{\sqrt{\sum\limits_{i=1}^{M} r_a^2(k) / M}} \quad (38)$$

$$\text{RME} = \frac{\max |r_a(k) - y_a(k)|}{\max |r_a(k)|} \quad (39)$$

where M represents the tested signal length. Referring to (38) and (39), the computed RMSE and RME indexes of different controllers for the tested random acceleration signal are given in Table 4 and Table 5. As indicated by Table 4 and Table 5, the RMSE index for TVC controller, parametric inverse compensator, and the proposed controller are 127.06%, 88.16% and 50.20%, while the RME index for these controllers are 148.62%, 92.03%

TABLE 4. RMSE of different controllers with random input.

Description	Input RMS	Error RMS	RMSE index
TVC controller	0.0653g	0.0830g	127.06%
Inverse compensator	0.0653g	0.0576g	88.16%
Proposed controller	0.0653g	0.0328g	50.20%

TABLE 5. RME of different controllers with random input.

Description	Max. Acc.	Max. Err.	RME index
TVC controller	0.2347g	0.3488g	148.62%
Inverse compensator	0.2347g	0.2160g	92.03%
Proposed controller	0.2347g	0.1156g	49.25%

and 49.25%, respectively. The computed quantitative indexes also reveal the feasibility of the proposed controller.

Apart from the tested random acceleration signal, a recorded earthquake wave, which happened in Westmorland in 1981, is also utilized to further analyze the validation of the proposed controller, and the time-history waveform for the recorded earthquake wave is depicted in Fig. 18. Applying the reference earthquake wave to the unidirectional EHST system, the experimental results of different controller are acquired in advance, and then the partial enlargement for acceleration waveforms together with the corresponding real-time tracking errors are presented in Fig. 19 and Fig. 20, respectively.
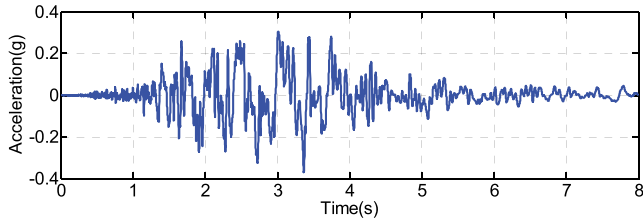
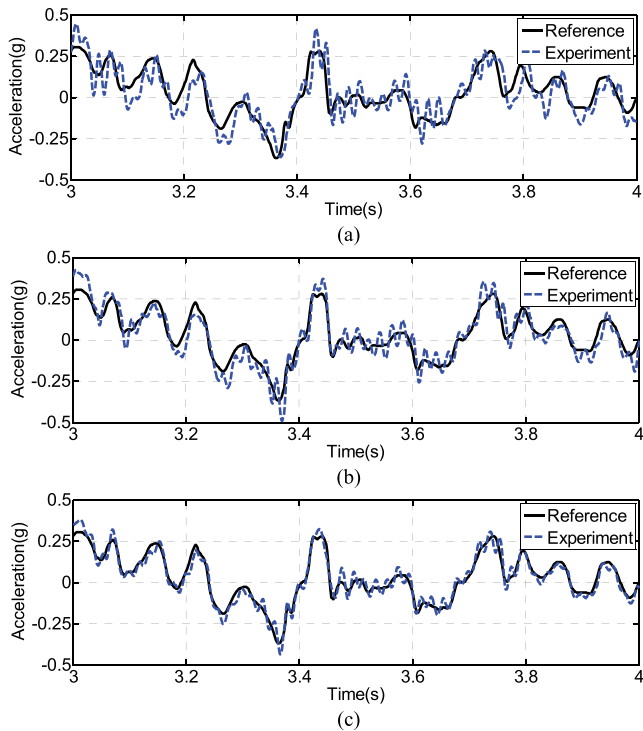**FIGURE 18.** Westmorland earthquake acceleration signal for EHST system.

FIGURE 19. Partial enlargement for different controllers with earthquake input. (a) TVC controller. (b) Parametric inverse compensator. (c) Proposed controller.

FIGURE 20. Tracking error of different controllers with earthquake input. (a) TVC controller. (b) Parametric inverse compensator. (c) Proposed controller.

TABLE 6. RMSE of different controllers with earthquake acceleration.

Description	Input RMS	Error RMS	RMSE index
TVC controller	0.0837g	0.0701g	83.79%
Inverse compensator	0.0837g	0.0497g	59.31%
Proposed controller	0.0837g	0.0337g	40.25%

TABLE 7. RME of different controllers with earthquake acceleration.

Description	Max. Acc.	Max. Err	RME index
TVC controller	0.3680g	0.2958g	80.38%
Inverse compensator	0.3680g	0.1728g	46.96%
Proposed controller	0.3680g	0.1335g	36.28%

As can be inferred from Fig. 19 and Fig. 20, the acceleration replication accuracy is limited by the traditional TVC controller, and with parametric inverse compensator the tracking performance is enhanced for either magnitude or phase property. Compared with these two controllers, the most prominent acceleration control result is achieved using the proposed adaptive control strategy.

For quantitive comparison purpose, the RMSE and the RME indexes for different controllers with recorded earthquake input signal are computed by (38) and (39), and the eventual obtained results are exhibited in Table 6 and Table 7. As can be observed from Table 6 and Table 7, the computed RMSE index for traditional TVC controller, parametric inverse compensator and the proposed controller are 83.79%, 59.31% and 40.25%, while the RME index for these controllers are 80.38%, 46.96% and 36.28% respectively, which again indicates that the proposed controller has a more superior tracking accuracy than the other comparative controllers.
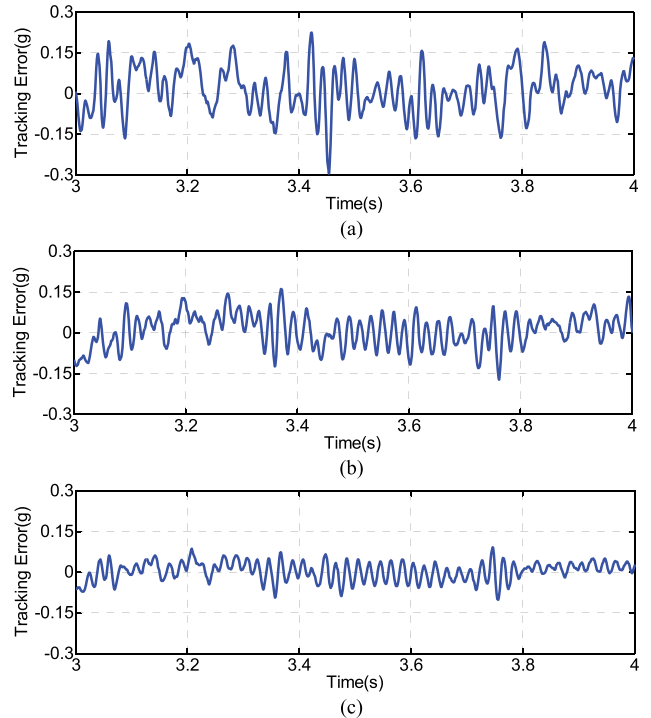
V. CONCLUSIONS

Aimed at improving the acceleration tracking performance of a unidirectional EHST system, this paper investigates a novel control strategy combining the parametric inverse compensation technique and the neural-based adaptive controller. The discrete system transfer function of the traditional TVC controlled EHST system is identified by the MISG algorithm in advance, and then ZMET technique is applied to the identified transfer function for a stable and casual inverse model. The parametric inverse compensation technique is constructed by cascading the designed inverse model to the traditional TVC controlled system. To handle the defects for the offline designed controllers, a neural-based adaptive controller including input, hidden and output

nodes is further incorporated as an outer loop, and the system's nonlinearities, varying dynamics and unexpected disturbances are effectively addressed. Finally, comparative experiments are carried out on a unidirectional EHST test rig with a random reference acceleration testing signal and a real recorded earthquake wave. The eventual experimental results indicate that the proposed acceleration control strategy produces more accurate table accelerations in contrast to the other comparative controllers.

ACKNOWLEDGMENT

REFERENCES

[1] M. Ahmadizadeh, G. Mosqueda, and A. M. Reinhorn, "Compensation of actuator delay and dynamics for real-time hybrid structural simulation," *Earthquake Eng. Struct. D*, vol. 37, no. 1, pp. 21–42, 2008.

[2] S. Pagano, M. Russo, S. Strano, and M. Terzo, "A mixed approach for the control of a testing equipment employed for earthquake isolation systems," *Proc. Inst. Mech. Eng., C, J. Mech. Eng. Sci.*, vol. 228, no. 2, pp. 246–261, 2013.

[3] A. R. Plummer, "Control techniques for structural testing: A review," *Proc. Inst. Mech. Eng., C, J. Syst. Control Eng.*, vol. 221, no. 2, pp. 139–169, 2007.

[4] A. Plummer, "A general co-ordinate transformation framework for multi-axis motion control with applications in the testing industry," *Control Eng. Pract.*, vol. 18, no. 6, pp. 598–607, 2010.

[5] R. Severn, "The development of shaking tables-a historical note," *Earthquake Eng. Struct.*, vol. 40, no. 2, pp. 195–213, 2011.

[6] S. A. Neild, D. P. Stoten, D. Drury, and D. J. Wagg, "Control issues relating to real-time substructuring experiments using a shaking table," *Earthquake Eng. Struct. D*, vol. 34, no. 9, pp. 1171–1192, 2005.

[7] T. Yu, Z. Zhencai, S. Gang, and L. Xiang, "Experimental investigation of feedforward inverse control with disturbance observer for acceleration tracking of electro-hydraulic shake table," *J. Vibroeng.*, vol. 17, no. 1, pp. 330–345, 2015.

[8] J. Yao and W. Deng, "Active disturbance rejection adaptive control of hydraulic servo systems," *IEEE Trans. Ind. Electron.*, vol. 64, no. 10, pp. 8023–8032, Oct. 2017, doi: 10.1109/TIE.2017.2694382.

[9] C. Wang, Z. Jiao, S. Wu, and Y. Shang, "Nonlinear adaptive torque control of electro-hydraulic load system with external active motion disturbance," *Mechatronics*, vol. 24, no. 1, pp. 32–40, 2014.

[10] J. Yao, R. Xiao, S. Chen, D. Di, S. Gao, and H. Yu, "Acceleration harmonic identification algorithm based on the unscented Kalman filter for shaking signals of an electro-hydraulic servo shaking table," *J. Vibrat. Control*, vol. 21, no. 16, pp. 3205–3217, 2015.

[11] J. P. Conte and T. L. Trombetti, "Linear dynamic modeling of a uniaxial servo hydraulic shaking table system," *Earthquake Eng. Struct. D*, vol. 29, no. 9, pp. 1375–1404, 2015.

[12] J. Yao, W. Deng, and Z. Jiao, "RISE-based adaptive control of hydraulic systems with asymptotic tracking," *IEEE Trans. Autom. Sci. Eng.*, vol. 14, no. 3, pp. 1524–1531, Jul. 2017.

[13] N. Nakata, "Acceleration trajectory tracking control for earthquake simulators," *Eng. Struct.*, vol. 32, no. 8, pp. 2229–2236 2010.

[14] G.-F. Guan, H.-T. Wang, and W. Xiong, "Random vibration control of a hydraulic shaking table," *J. Vibrat. Control*, vol. 20, no. 2, pp. 204–217, 2014.

[15] R. F. Nowak, D. A. Kusner, R. L. Larson, and B. K. Thoen, "Utilizing modern digital signal processing for improvement of large scale shaking table performance," in *Proc. WCEE*, 2000, pp. 2035–2043.

[16] J. Yao, W. Deng, and Z. Jiao, "Adaptive control of hydraulic actuators with lugre model-based friction compensation," *IEEE Trans. Ind. Electron.*, vol. 62, no. 10, pp. 6469–6477, Oct. 2015.

[17] J. Yao, Z. Jiao, and D. Ma, "A practical nonlinear adaptive control of hydraulic servomechanisms with periodic-like disturbances," *IEEE/ASME Trans. Mechatronics*, vol. 20, no. 6, pp. 2752–2760, Dec. 2015.

[18] S. Strano and M. Terzo, "A SDRE-based tracking control for a hydraulic actuation system," *Mech. Syst. Signal Process.*, vols. 60–61, pp. 715–726, Aug. 2015.

[19] J. Yao and W. Deng, "Active disturbance rejection adaptive control of uncertain nonlinear systems: Theory and application," *Nonlinear Dyn.*, vol. 89, no. 3, pp. 1611–1624, 2017.

[20] J. Yao, W. Deng, and W. Sun, "Precision motion control for electro-hydraulic servo systems with noise alleviation: A desired compensation adaptive approach," *IEEE/ASME Trans. Mechatronics*, vol. 22, no. 4, pp. 1859–1868, Apr. 2017.

[21] Y. Tagawa and K. Kajiwara, "Controller development for the e-defense shaking table," *Proc. Inst. Mech. Eng., C, J. Syst. Control Eng.*, vol. 221, no. 2, pp. 171–181, 2007.

[22] B. Spencer, Jr., and G. Yang, "Earthquake simulator control by transfer function iteration," in *Proc. ASCE-EM*, 1998, pp. 17–20.

[23] J. D. Cuyper, M. Verhaegen, and J. Swevers, "Off-line feed-forward and H_∞ feedback control on a vibration rig," *Control Eng. Pract.*, vol. 11, no. 2, pp. 129–140, 2003.

[24] J. De Cuyper, D. Vaes, W. Dehandschutter, J. Swevers, M. Verhaegen, and P. Sas, "Experimental H_∞ control to improve an industrial off-line tracking control scheme on an automotive suspension test rig," in *Proc. CACSD*, 2002, pp. 63–68.

[25] B. S. Twitchell and M. D. Symans, "Analytical modeling, system identification, and tracking performance of uniaxial seismic simulators," *J. Eng. Mech.*, vol. 129, no. 12, pp. 1485–1488, 2003.

[26] Y. Tang, G. Shen, Z. C. Zhu, X. Li, and C. F. Yang, "Time waveform replication for electro-hydraulic shaking table incorporating off-line iterative learning control and modified internal model control," *Proc. Inst. Mech. Eng., C, J. Syst. Control Eng.*, vol. 228, no. 9, pp. 722–733, 2014.

[27] D. P. Stoten and E. G. Gómez, "Adaptive control of shaking tables using the minimal control synthesis algorithm," *Philos Trans. R. Soc. A*, vol. 359, no. 1786, pp. 1697–1723, 2001.

[28] D. Stoten and N. Shimizu, "The feedforward minimal control synthesis algorithm and its application to the control of shaking-tables," *Proc. Inst. Mech. Eng., C, J. Syst. Control Eng.*, vol. 221, no. 3, pp. 423–444, 2007.

[29] A. Gizatullin and K. Edge, "Adaptive control for a multi-axis hydraulic test rig," *Proc. Inst. Mech. Eng., C, J. Syst. Control Eng.*, vol. 221, no. 2, pp. 183–198, 2007.

[30] J. Yao, D. Di, G. Jiang, and S. Gao, "Acceleration amplitude-phase regulation for electro-hydraulic servo shaking table based on LMS adaptive filtering algorithm," *Int. J. Control*, vol. 85, no. 10, pp. 1581–1592, 2012.

[31] K. Seki, M. Iwasaki, M. Kawafuku, H. Hirai, and K. Yasuda, "Adaptive compensation for reaction force with frequency variation in shaking table systems," *IEEE Trans. Ind. Electron.*, vol. 56, no. 10, pp. 3864–3871, Oct. 2009.

[32] S. Gang *et al.*, "Adaptive feed-forward compensation for hybrid control with acceleration time waveform replication on electro-hydraulic shaking table," *Control Eng. Pract.*, vol. 21, no. 8, pp. 1128–1142, 2013.

[33] M. Stehman and N. Nakata, "Direct acceleration feedback control of shake tables with force stabilization," *J. Earthquake Eng.*, vol. 17, no. 5, pp. 736–749, 2013.

[34] B. M. Phillips, N. E. Wierschem, and B. F. Spencer, "Model-based multi-metric control of uniaxial shake tables," *Earthquake Eng. Struct.*, vol. 43, no. 5, pp. 681–699, 2014.

[35] T. Y. Yang, K. Li, J. Y. Lin, Y. Li, and D. P. Tung, "Development of high-performance shake tables using the hierarchical control strategy and nonlinear control techniques," *Earthquake Eng. Struct.*, vol. 44, no. 11, pp. 1717–1728, 2015.

[36] L. Zhang, D. Cong, Z. Yang, Y. Zhang, and J. Han, "Robust tracking and synchronization of double shaking tables based on adaptive sliding mode control with novel reaching law," *IEEE Access*, vol. 4, pp. 8686–8702, 2016.

[37] H. E. Merritt, *Hydraulic Control Systems*. New York, NY, USA: Wiley, 1967, pp. 150–152.

[38] F. Ding and T. Chen, "Performance analysis of multi-innovation gradient type identification methods," *Automatica*, vol. 43, no. 1, pp. 1–14, 2007.

[39] J. A. Butterworth, L. Y. Pao, and D. Y. Abramovitch, "Analysis and comparison of three discrete-time feedforward model-inverse control techniques for nonminimum-phase systems," *Mechatronics*, vol. 22, no. 5, pp. 577–587, 2012.

[40] M. A. Vaudrey, W. T. Baumann, and W. R. Saunders, "Stability and operating constraints of adaptive LMS-based feedback control," *Automatica*, vol. 39, no. 4, pp. 595–605, 2003.

[41] F. Bonsignorio and A. Del Pobil, "Toward replicable and measurable robotics research [from the guest editors]," *IEEE Robot. Autom. Mag.*, vol. 22, no. 3, pp. 32–35, Mar. 2015.

[42] J. Mattila, J. Koivumäki, D. G. Caldwell, and C. Semini, "A survey on control of hydraulic robotic manipulators with projection to future trends," *IEEE/ASME Trans. Mechatronics*, vol. 22, no. 2, pp. 669–680, Feb. 2017.

GANG SHEN received the B.S. degree from Jiamusi University in 2005, the M.S. and Ph.D. degrees from the Harbin Institute of Technology, in 2007 and 2011, respectively. He is currently a Professor with the School of Mechanical and Electrical Engineering, China University of Mining and Technology. His research interests include electro-hydraulic servo control, parallel robot, and loading systems.

YU TANG received the B.S. and Ph.D. degrees from the China University of Mining and Technology in 2011 and 2016, respectively. He is currently a Lecturer with the School of Mechanical and Electrical Engineering, China University of Mining and Technology. His research interests include electro-hydraulic servo control, acceleration control, and force control.

ZHENCAI ZHU received the B.S., M.S., and Ph.D. degrees from the China University of Mining and Technology in 1989, 1994, and 2000, respectively. He is currently a Professor with the School of Mechanical and Electrical Engineering, China University of Mining and Technology, where he is also the Executive Vice-Dean with the Research Academy. His research interests include mechanical system control and impact dynamics.

WENJUAN ZHANG received the B.S. and M.S. degrees from the China University of Mining and Technology in 2011 and 2014, respectively. She is an Experimentingist with the School of Mechanical and Electrical Engineering, China University of Mining and Technology. Her research interests include electro-hydraulic system control.

● ● ●